has been used to derive an equation for the kinetics under conditions where mobility data are unavailable. With this model, a value of 400 ± 30 μF cm^{-2} for the iron oxide inner-layer capacitance has been calculated, using only kinetic data.

Appendix

The surface potential of a Nernstian oxide[14] at 25 °C is given by

$$\Psi_0 = 0.0592(\text{pzc} - \text{pH}) \quad \text{(A1)}$$

According to the ZOS model,[14] the double layer can be broken up into an inner Helmholtz layer, of fixed integral capacitance K_I and dielectric constant ϵ_I, and a diffuse layer of capacitance K_d. The ZOS model postulates that the Helmholtz layer is a region devoid of charge and of thickness β. The outer Helmholtz plane (OHP) is then the start of the diffusion layer, and the potential at the OHP is also assumed to be identical with the experimentally observed ζ potential. In the absence of specific ion adsorption, the condition of charge neutrality for the interface is that the surface charge, σ_0, is balanced by the charge in the diffuse layer, σ_d. Then

$$\sigma_0 = -\sigma_d \quad \text{(A2)}$$

The potential gradient in the inner region is linear, so the potential at the OHP, which is also the plane of electron transfer, must be given by

$$\zeta = \Psi_0 - \sigma_0/K_I = \Psi_0 + \sigma_d/K_I \quad \text{(A3)}$$

For particles in the size range 30–100 Å, the condition $d \ll a$ still holds, and the flat plate condenser model for the inner layer is justified. However, the diffuse layer thickness characterized by the Debye–Hückel parameter κ^{-1} is now much larger than a. The diffuse layer must be considered spherical as outlined in the earlier part of this paper. Ohshima et al.[16] showed that for a sphere of radius a immersed in a 1:1 electrolyte of Debye–Hückel length κ^{-1}

$$\frac{\sigma_0 e}{\epsilon\epsilon_0 \kappa k T} = 2 \sinh (e\zeta/2kT) \times \left[1 + \frac{2}{A \cosh^2 (e\zeta/4kT)} + \frac{8 \ln [\cosh (e\zeta/4kT)]}{A^2 \sinh^2 (e\zeta/2kT)}\right]^{1/2} \quad \text{(A4)}$$

where $A = \kappa a$.

Equations A3 and A4 provide two equations for ζ as a function of σ_0, which can be readily solved numerically by using the experimental values a, κ, and Ψ_0 and fitting K_I as the only adjustable parameters. The curves in Figure 2a,b are both fitted with the same $K_I = 400$ μF cm^{-2}.

Acknowledgment. Many thanks to Derek Chan and Stan Miklavic for their advice and for many useful discussions. P.M. acknowledges the receipt of a Commonwealth Postgraduate Award. Work at ANL was performed under the auspices of the Office of Basic Energy Sciences, Division of Chemical Science, US-DOE under contract no. W-31-109-ENG-38. A grant from the Australian Institute of Nuclear Science and Engineering to the University of Melbourne is gratefully acknowledged. The dedication of the ANL linac operators is much appreciated.

Registry No. MV^{2+}, 4685-14-7; ZV$^-$, 79008-86-9; FeO (unspecified), 1332-37-2.

(16) Ohshima, H.; Healy, T. W.; White, L. R. *J. Colloid Interface Sci.* **1982**, *90*, 17.

Evolution of Chemically Induced Unstable Density Gradients Near Horizontal Reactive Interfaces

Ofra Citri,[†,‡] Michael L. Kagan,[†,‡] Ronnie Kosloff,[*,‡] and David Avnir[*,†,‡]

Department of Organic Chemistry and the F. Haber Research Center for Molecular Dynamics, The Hebrew University, Jerusalem 91904, Israel

Received July 27, 1989

We study the evolution of concentration and density profiles in the course of chemical reactions near horizontal interfaces. Examples include first-order reaction with a catalytic surface, second-order reaction in a double-diffusive liquid–liquid interface, gas–liquid or liquid–membrane–liquid reactions, and the irradiation of a photoactive liquid interface. Our main observation is that, quite often, the resulting density profiles indicate potentially unstable hydrodynamic configurations that may lead to mass distribution through spontaneous convections, i.e., much faster than diffusion.

1. Introduction[1]

Hydrodynamic instability in liquids near interfaces may evolve whenever gradients of temperature, surface tension, or concentrations build up.[2] Despite the fact that all these gradients can be induced by a chemical reaction, *chemical* routes to such instabilities are significantly less explored than physical routes. There are, however, a number of important contributions to this topic; most of them concentrate on instabilities which origi-

† Department of Organic Chemistry.

‡ F. Haber Research Center for Molecular Dynamics.

(1) A preliminary partial version appeared in *Synergetics, Order and Chaos*; Velarde, M. G., Ed.; World Scientific, 1988; p 292.

(2) Chandrasekhar, S. *Hydrodynamic and Hydrodynamic Stability*; Dover: New York, 1981.

0743-7463/90/2406-0559$02.50/0

nate from Marangoni free-surface deformations,[3] i.e., from horizontal surface tension inhomogeneities. From these studies, we notice especially the theoretical studies of chemo-Marangoni instabilities,[4] the dissociating liquid problem studies by Frisch et al.[5] and by Lopushausleaya et al.,[6] studies on thermal convections in photochemical systems[7] and in chemical waves,[8] and the study of Selva et al.[9] on hydrodynamic fluctuations in chemically reactive fluid.

The simulation study reported here rests particularly on our general observation that the reaction product which is formed in a wide variety of chemical reactions through horizontal liquid interfaces is distributed throughout the bulk by convective modes.[10,11] Our study focused on reaction configurations in which the interface is not free, thus excluding the Marangoni mechanism,[12] and the cause for the phenomenon was identified as unstable vertical density gradients.[10,13] The main consequence of these observations is that reaction kinetics near horizontal interfaces cannot be analyzed only in terms of slow diffusion mechanisms and that spontaneous convective mass transport may dominate such systems.

To understand how a reaction may induce convections, consider the following: When a reaction occurs at or through the top surface, the reactants develop stable density gradients (their concentrations decrease upward) and the products develop unstable density gradients (concentrations increase upward). When the reaction occurs on the bottom surface, the situation is, of course, reversed. In both cases, the combination of opposing vertical density gradients may then lead to an overall unstable profile which, above a critical point, will develop into convections.

To demonstrate these ideas and to show the generality of the phenomenon, we present in the following sections several examples of concentration and density profiles that are generated during chemical reactions near an interface. We show that under conditions of constant temperature and pressure, where the resulting density gradients are due only to the vertical concentration profiles of reactants and products, the potentially unstable situation of top-heavy on bottom-light is observed in many cases. We begin with two-component systems, continue with somewhat more complex three-component systems, and conclude with simulations of a photochemical reaction of a reactive liquid. In the latter case, we were also able to detect experimentally the bifurcation point from the homogeneous diffusive regime into the (spectacular) patterned convective mode.[10] Yet we do not attempt in this report to identify the point of collapse of the density gradients in the time domain, not only because we are unaware of any practical approximation to calculate critical Rayleigh values for the type of complex profiles reported here but also because the moment of collapse depends very much on the rate at which the instability is reached[14] (by analogy to the freezing of a supercooled liquid). Yet, as mentioned above, we regard it of importance to report our observations due to their potential implication on reaction kinetics near catalytic and noncatalytic interfaces.

2. Details of the Calculations

The partial differential equations describing a reaction/diffusion system have the general form

$$\frac{\partial C_i}{\partial t} = D_i \nabla^2 C_i + \text{reaction terms} \tag{1}$$

where C_i and D_i are the concentration and the diffusion coefficient of species i respectively. (We ignore the cross terms D_{ij}.)

For some of the simulations below, the boundary condition is impermeability to mass at the rigid walls of the vessel, i.e.:

$$\frac{\partial C_i}{\partial x} = 0 \text{ at } x = 0, x = L \tag{2}$$

The density of the solution as a function of the distance from the interface is

$$\rho(x) = \rho_0(1 + \sum \alpha_i C_i(x)) \tag{3}$$

where ρ_0 is the density of pure solvent and α_i is the concentration expansion coefficient of species i, defined as

$$\alpha_i = \frac{1}{\rho}\frac{\partial \rho}{\partial C_i} \tag{4}$$

Since we are only interested in density differences, the calculation in the following is given as normalized $\Delta\rho$:

$$\Delta\rho = \frac{\rho - \rho_0}{\rho_0} \tag{5}$$

The equations were numerically integrated on a one-dimensional grid. (As long as there are no convections, the system is homogeneous in y and z; thus there is no need to work in a higher dimension.) To solve the equations of type (1), we have used the pseudospectral method recently developed by Kosloff and Kosloff[15] as explained in detail in ref 16. The propagation in time is done by a simple Euler method, and the gradients are calculated after each time step by fast Fourier transform (FFT). In order to satisfy the boundary condition (2), the number of the grid cells is doubled and the concentrations are reflected about one edge (such that $C(i) = C(2n + 1 - i)$) before each operation of the Laplacian. Because of the periodic nature of FFT, this is equivalent to total reflecting walls.

(3) (a) Nakache, E.; Duperyat, M.; Vignes-Adler, M. J. *J. Colloid. Interface Sci.* **1983**, *94*, 187. (b) Frenzel, G.; Linde, H. ref 1, p 158 and other articles in section F.

(4) Defay, R.; Prigogine, I.; Safeld, A. *Colloid Interface Sci.* **1977**, *1*, 527. Ibanez, J. L.; Velarde, M. G. *J. Phys.* **1977**, *38*, 1479. Sorensen, T. S.; Hennenberg, M.; Steinchen-Sanfeld, A.; Sanfeld, A. *Prog. Colloid Interface Sci.* **1976**, *61*, 64. Ruckerstein, E.; Berbente, C. *Chem. Eng. Sci.* **1964**, 19. Pismen, L. M. *J. Colloid Interface Sci.* **1984**, *102*, 11. Vedove, W. D.; Bisch, P. M. *J. Phys. (Les Ulis, Fr.)* **1982**, *43*, 1. Dagan, Z.; Pismen, L. M. *J. Colloid Interface Sci.* **1984**, *99*, 215.

(5) Bdzil, J. B.; Frisch, H. L. *J. Chem. Phys.* **1980**, *72*, 1875. Wollkind, D. J.; Frisch, H. L. *Phys. Fluids* **1971**, *14*, 13. Bdzil, J. B.; Frisch, J. B. *Ibid.* **1971**, *14*, 107.

(6) Lopushanskaya, A. I. et al. *Russ. J. Phys. Chem.* **1973**, *47*, 1418.

(7) Gutkowiticz-Krusin, D.; Ross, J. *J. Chem. Phys.* **1980**, *72*, 3577. Epstein, I. R.; Morgan, M.; Steel, C.; Valdes-Aguilera, O. *J. Phys. Chem.* **1983**, *87*, 3955. Pearlstein, A. I. *J. Chem. Phys.* **1985**, *89*, 1054.

(8) Bazsa, G.; Epstein, I. R. *J. Phys. Chem.* **1985**, *89*, 3050. Nagypal, I.; Bazsa, G.; Epstein, I. R. *J. Am. Chem. Soc.* **1986**, *108*, 3635. Milke, H.; Muller, S. C.; Hess, B. *Chem. Phys. Lett.* **1988**, *144*, 515.

(9) de la Selva, S. M. T.; Garcia-Colin, L. S. *J. Chem. Phys.* **1986**, *85*, 2140.

(10) (a) Avnir, D.; Kagan, M. L. *Nature* **1984**, *307*, 717. (b) Avnir, D.; Kagan, M. L.; Ross, W. *Chem. Phys. Lett.* **1987**, *135*, 177 and references cited therein. (c) Heidel, B.; Knobler, C. M.; Hilfer, R.; Bruinsma, R. *Phys. Rev. Lett.* **1988**, *60*, 2492.

(11) Bowers, P. G.; Solzberg, L. J. *J. Chem. Ed.* **1989**, *66*, 210.

(12) Gimenez, M.; Micheau, J. C. *Naturwissenschaften* **1983**, *70*, 90. Micheau, J. C.; Gimenez, M.; Brockmans, P.; Dewel, G. *Nature* **1983**, *305*, 43.

(13) Kagan, M. L. *Chemical Formation of Dissipative Spatial Structures*; Ph.D. Thesis, The Hebrew University of Jerusalem, 1988.

(14) Mahler, E. G.; Schechter, R. S.; Wissler, E. H. *Phys. Fluids* **1968**, *11*, 1901.

(15) Kosloff, D.; Kosloff, R. *J. Comput. Phys.* **1983**, *52*, 35. Kosloff, R. *J. Phys. Chem.* **1988**, *92*, 2087.

(16) Kagan, M. L.; Kosloff, R.; Citri, O.; Avnir, D. *J. Phys. Chem.* **1989**, *93*, 2728.

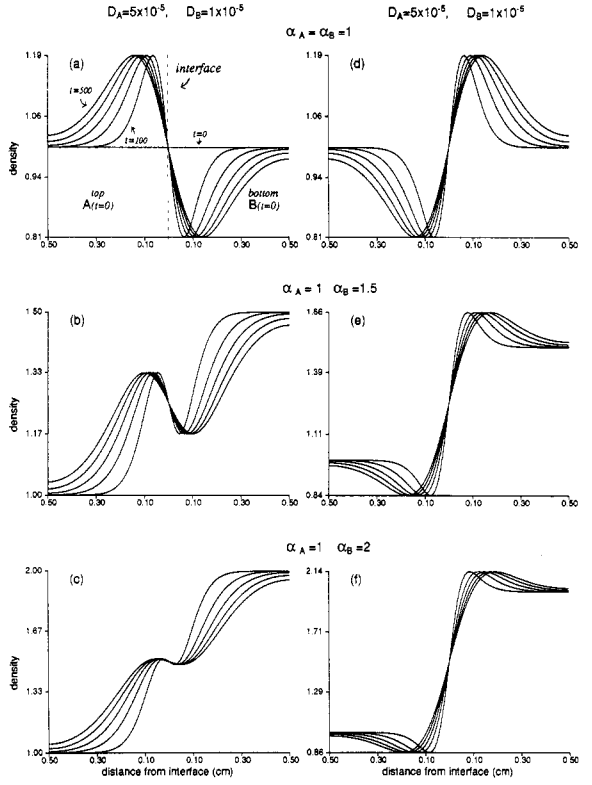

Figure 1. Evolution of density profiles in a double-diffusion system without a reaction. At time = 0 the interface between the solutions is located at $x = 0$. The x axis gives the distance from the initial interface. (a–c) $D_A = 5 \times 10^{-5}$, $D_B = 1 \times 10^{-5}$ cm^2/s; (d–f) $D_A = 1 \times 10^{-5}$, $D_B = 5 \times 10^{-5}$ cm^2/s. The expansion coefficients are given in the figure. Density profiles are given every 100 s. At t = 100 s the unstable region expands between approximately 0.2 cm from left to 0.1 cm to the right of the initial interface. The details in Figure 1a are applicable to all figures below.

3. Results

1. Double Diffusion with and without Reaction. We begin with an introductory case which does not involve a reaction: A layer of solution A is on top of solution B. The two solutions have a common solvent but different solutes A and B. We consider only cases where $\alpha_A C_{A_0} \leq \alpha_B C_{B_0}$, where C_{A_0} and C_{B_0} are the initial concentration of A and B respectively, i.e., when the top solution is initially lighter than or has the same density as the bottom solution. For computation convenience, we define $\alpha_A C_{A_0} = 1$, without losing generality.

Figure 1 shows the evolution of density profiles with time for two sets of diffusion coefficients. When $D_A < D_B$ (Figure 1a–c), the upper layer is enriched with B faster than it loses A, and density inversion occurs around the initial interface. As α_B increases (1a → 1b → 1c), the relative weight of the stable part increases, and when B is much heavier than A (1c), the unstable gradient disappears.

When $D_A > D_B$ (Figure 1d–f), the diffusion of B into the upper layer does not compensate for the "escaping" of A and no inversion occurs, but the stable layer around the interface is bounded by unstable gradients. As the ratio $C_{A_0}\alpha_A / C_{B_0}\alpha_B$ decreases, the relative part of the unstable part decreases too.

In the purely double-diffusion case, where neither consumption of starting materials nor generation of new products occurs, the absolute value of the density difference is reached immediately after diffusion starts and does not change with time (as long as the components do not reach the opposite wall), as can be seen clearly in Figure

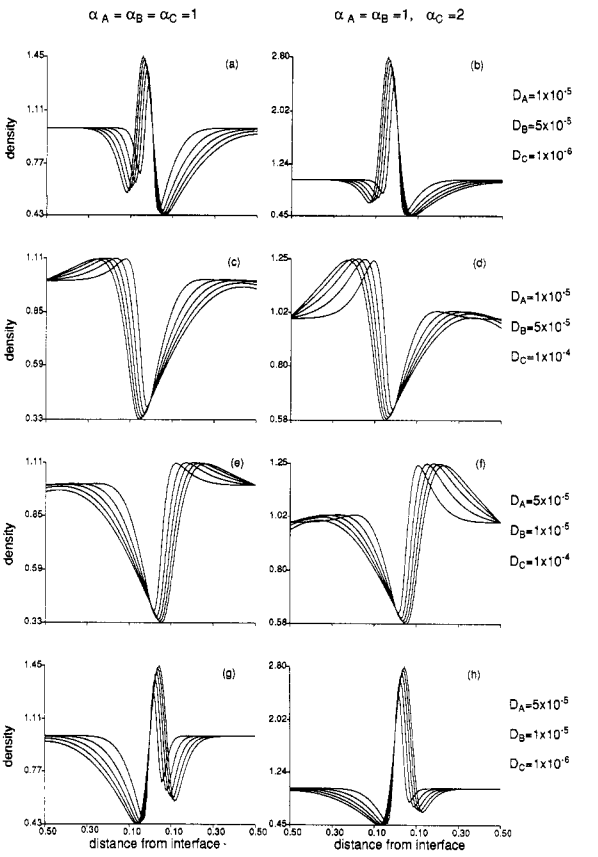

Figure 2. Evolution of density profiles for double diffusion with a reaction, $k = 10$ s^{-1}. Diffusion coefficients are given on the right of each pair of profiles (a–b, c–d, etc.). The two sets of expansion coefficients are given above and are common to each column. Profiles are given every 100 s.

1. The only change with time is the thickness of the layer over which this difference expands. This difference is determined by the ratio between the diffusion coefficients. Unlike this case, where reaction does take place, both the density difference and the layer thickness are growing with time. In some of these cases, however, they evolve on different time scales, and the density difference reaches its maximum within a short period after the reaction begins. This will be demonstrated in the following examples.

We now impose on this double-diffusion system the simple reaction:

$$A + B \xrightarrow{k} C \qquad (6)$$

The picture, as seen in Figure 2, changes dramatically. For the two sets of D_A and D_B of Figure 1 (and for $\alpha_A = \alpha_B = \alpha_C = 1$), one can see that if the diffusion of C is faster than that of A and B, the density has a minimum around the initial interface (Figure 2c–f), and if it is slower, the density has a maximum (Figure 2a,b,g,f). The addition of a third component around the initial interface increases the number of extrema in the density, and now there is always a region of unstable density gradient. In comparison with Figure 1, the solution is now more susceptible to convections. Changing the expansion coefficient of C does not change the density profile shape but only its magnitude (compare the pairs a–b, c–d, etc., in Figure 2).

2. First-Order Reaction with a Catalytic Surface. In this section, we study the simple first-order reaction

$$A \xrightarrow{k} B \qquad (7)$$

catalyzed by a horizontal catalytic wall, A, which is initially contained in a homogeneous solution of depth L, diffuses to a catalytic wall, and is converted to B. As the reaction starts, concentration gradients are formed that cause A to diffuse toward the interface and B to diffuse from the interface into the bulk. In the model, we ignore any complications that might arise from the coverage of the interface and assume that all stages of the reaction may be represented by one isothermal first-order reaction.

The differential equations governing the system are

$$\partial A/\partial t = -k(x)A + D_A\nabla^2 A \tag{8a}$$

$$\partial B/\partial t = k(x)A + D_B\nabla^2 B \tag{8b}$$

where k, the reaction rate constant, vanishes to zero at a small distance from the interface and D_A and D_B are the diffusion coefficients of A and B, respectively. A_0 and $B_0 = 0$ are the initial homogeneous concentrations of A and B, respectively.

Figure 3 shows the evolution of the concentration profiles as a function of the diffusion coefficients for $k = 10$ s^{-1}. With this rate constant, the reaction is fast enough so that the concentration of A near the wall drops to zero after a few seconds. It can be seen that, as expected, the higher diffusion coefficients are associated with flatter profiles, i.e., with deeper penetration and lower concentration difference.

At the limit of very fast reaction (diffusion-controlled reaction), the concentration of A on the wall is 0, and eq 8 have an analytic solution[17]

$$A(x) = A_0 \,\mathrm{erf}\ (x/2(D_A t)^{1/2})$$

$$B(x) = A_0(D_A/D_B)^{1/2}\,\mathrm{erfc}\ (x/2(D_B t)^{1/2}) \tag{9}$$

At lower k values, the concentration profiles do not deviate much from a Gaussian centered at $x = 0$ (as long as the penetration depth is smaller than L) with a width proportional to $(Dt)^{1/2}$ (as in the simple diffusion problem) and at the limit of a very small k (reaction controlled). At moderate reaction times, the concentrations at the interface are

$$\Delta A(0) = A_0 - A(0) \propto kA_0(t/D_A)^{1/2}$$

$$B(0) \propto kA_0(t/D_B)^{1/2} \tag{10}$$

Figure 4 shows the changes in the density profiles as a function of the diffusion coefficients and of the ratio α_B/α_A. As can be seen, the overall shape of the density profile is quite sensitive to the ratio α_B/α_A: for all diffusion coefficient sets, it is seen that going from $\alpha_B > \alpha_A$ (top row) to $\alpha_B < \alpha_A$ (bottom row) the density profiles change from those resembling the concentrations profiles of B (see Figure 3) to those resembling A. Nonmonotonic profiles, i.e., those that are potentially unstable whether the catalyst is the top or the bottom wall, are formed when the expansion coefficients are comparable (center row).

3. Reaction between Solutions Separated by a Semipermeable Membrane or between a Gas and a Solution. In this subsection, we consider reaction 6 in a configuration where two solutions, A and B, are separated by a membrane permeable to A only or where A is a gas diffusing into a solution of B. If the reaction is very fast, i.e., B is converted immediately to C, the profiles resemble those of the catalytic case (section 4); if, however, the reaction is not so fast, all three components are present in the solution and contribute to the density profiles. The concentration profiles for $k = 10$ M^{-1} s^{-1} and an initial concentration of 10^{-3} M are shown in Figure 5. The resulting density profiles are shown in Figure 5. One can see that in contradistinction with this case the previous examples, both the magnitude of the density differences and the gradient width, change with time due to the evolution of the C profile (Figure 5c). Here, the density profiles are nonmonotonic; i.e., the solutions are potentially unstable whether the reaction occurs through the top or the bottom surface.

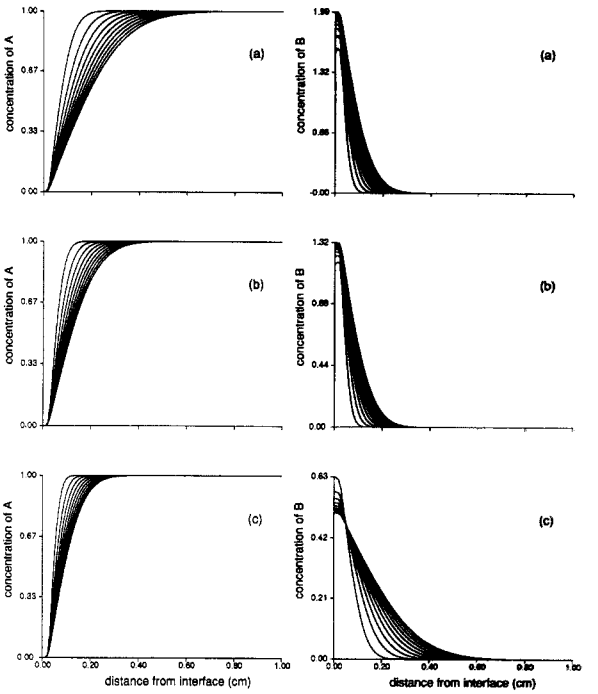

Figure 3. Time evolution of the concentration profiles of A and B for the catalytic reaction A → B as a function of the diffusion coefficients for $k = 10$ s^{-1}: (a) $D_A = 5 \times 10^{-5}$, $D_B = 1 \times 10^{-5}$ cm^2/s; (b) $D_A = 2 \times 10^{-5}$, $D_B = 1 \times 10^{-5}$ cm^2/s; (c) $D_A = 1 \times 10^{-5}$, $D_B = 5 \times 10^{-5}$ cm^2/s. Profiles shown are taken every 50 s. The first small extremum observed in the concentration profiles of A and B and in Figure 4 is due to the Gaussian form chosen for $k(x)$: $k(x) = k\exp(-x^2/\sigma^2)$; σ was chosen as 1×10^{-2} cm. The shape of the profiles, except very near the interface, is not affected much by the choice of σ.

4. Photochemical Reaction. As mentioned in the Introduction, intensive experimental work has been done in our laboratory and others concerning the photochemical reduction of Fe^{3+} to Fe^{2+} by oxalic acid and the formation of Turnbull's blue,[13] which leads to patterns and convections. The reaction was investigated under various conditions, and the onset of convections was found to be in all cases on the order of minutes.

The proposed kinetic model for the reaction is the following:[13] A and B ($FeCl_3$ and $K_3Fe(CN)_6$) are mixed in a large excess of the acid. Upon irradiation through the interface, A is excited and undergoes a very fast conversion to a reactive intermediate E, which then reacts with B, yielding the end product C ($KFeFe(CN)_6$: Turnbull's blue):

$$A \xrightarrow{h\nu} E$$

$$B + E \xrightarrow{k} C \tag{11}$$

(17) Byron, R.; Stewart, W. E.; Lightfoot, E. N. *Transport Phenomena*; Wiley: New York, 1965.

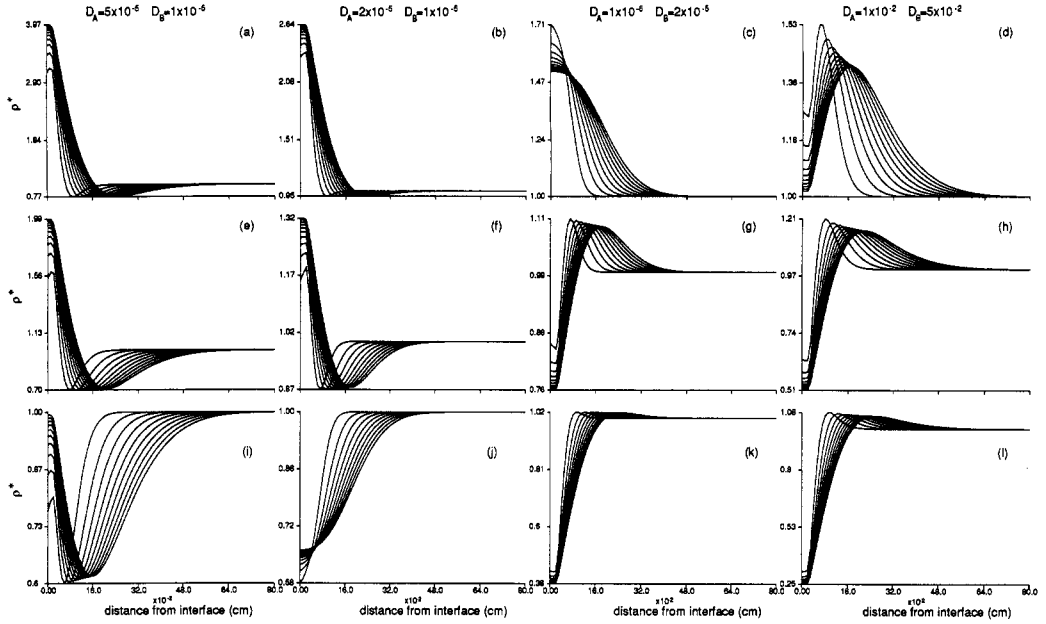

Figure 4. Evolution of density profiles (taken every 50 s) for the reaction of Figure 3 for four sets of diffusion coefficients and for different expansion coefficients ratios. (a–d) $\alpha_B/\alpha_A = 2$; (e–h) $\alpha_B/\alpha_A = 1$; (i–l) $\alpha_B/\alpha_A = 0.5$. The indicated diffusion coefficients refer to all profiles in the corresponding column.

The differential equations describing the system are

$$\partial A/\partial t = -I\epsilon_A A + D_A\nabla^2 A \tag{12}$$

$$\partial E/\partial t = I\epsilon_A A + D_E\nabla^2 E \tag{13}$$

$$\partial B/\partial t = -kBE + D_B\nabla^2 B \tag{14}$$

$$\partial C/\partial t = kBE + D_C\nabla^2 C \tag{15}$$

$$I(x) = I_0 e^{-\int_0^x(\epsilon_A A+\epsilon_B B+\epsilon_C C)dx} \tag{16}$$

where I_0 is the irradiation intensity, $I(x)$ the light intensity in the solution, and ϵ_i the extinction coefficients. The concentration of E is assumed to be sufficiently low so that its light absorption and contribution to the density profiles can be ignored.

Equations 12–16 were solved with the known set of experimental parameters[13] specified in Figure 6 for the initial parameters $C_{A_0} = C_{B_0} = 1.4 \times 10^{-2}$ M and $I_0 = 5.8 \times 10^{-9}$ photons/(s·cm^2). The experimental onset time for this set of conditions is about 5 min.

A special feature of this case results from the light intensity profile: A and B, which absorb light, are consumed, thus allowing deeper penetration of the light as the reaction proceeds. Consequently, the gradient's thickness is determined not only by the diffusion coefficients of the components but mostly by the light intensity profile. This feature can be seen by comparing the profiles of A and C, bearing in mind that their diffusities differ by 1 order of magnitude.

4. Discussion: Some Hydrodynamic Instability Considerations

Inspection of Figures 1–6 calls for the intuitive conclusion that at least some of the density profiles (e.g., Figure 1a, Figure 2c, Figure 4a, etc.) are prone for convective collapse. Although, as mentioned in the Introduction, we are unprepared at the moment to carry on the above calculations into the convective regime, we believe that some comments on that issue are in order.

In a one-component solution, the situation of heavy top on light bottom is a necessary (but not sufficient) condition for convections. The criteria for stability is

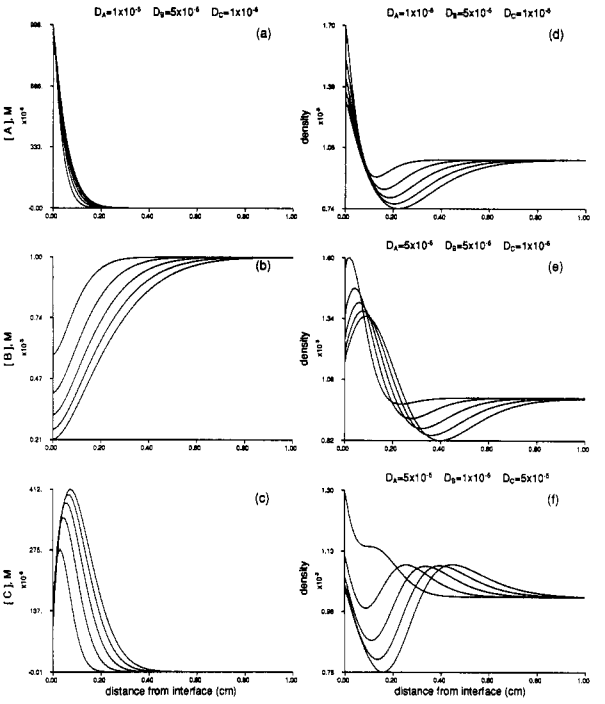

Figure 5. Evolution of concentration and density profiles for semipermeable membrane or for gas reacting with solution. The right column gives the concentration profiles for the set of diffusion coefficients given above the column. The left column gives density profiles for three different sets of diffusion coefficients, indicated above each figure. Expansion coefficients $\alpha_A = \alpha_B = \alpha_C = 1$, $k = 10$ s^{-1}.

the Rayleigh number, the balance between the stabilizing (diffusion and viscosity), and the destabilizing (gravitation) forces

$$Ra = \frac{g\alpha\Delta C h^3}{D\nu} \tag{17}$$

where g is the gravitation constant, ΔC the concentration difference, h the thickness of the unstable layer, and ν the viscosity. Depending on the boundary conditions (free, etc.), there is a critical value beyond which the solu-

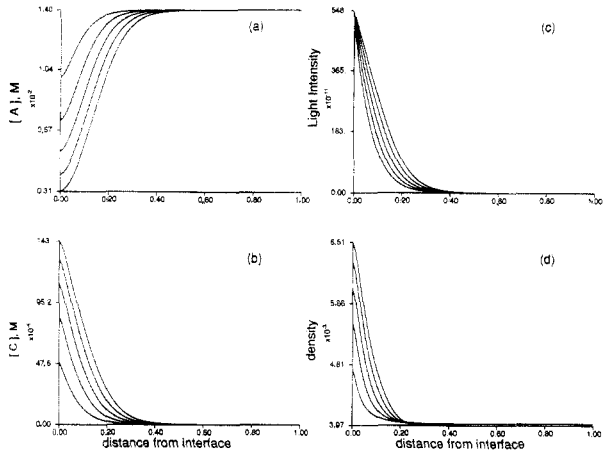

Figure 6. Evolution of concentration profiles (a,b) light intensity profile (c) and density profile (d) in the photochemical reaction 11 (section 3.4). The profiles are shown every 100 s after the reaction began. Parameters used for simulation: extinction coefficient, $\epsilon_A = 900$, $\epsilon_A = 320$, $\epsilon_A = 100$ M^{-1} cm^{-1}; diffusion coefficients, $D_E = 7 \times 10^{-6}$, $D_B = 9.4 \times 10^{-6}$, $D_C = 9.3 \times 10^{-7}$ cm^2/s; expansion coefficients, $\alpha_A = 0.14$, $\alpha_A = 0.145$, $\alpha_A = 0.395$ M^{-1}; $k = 100$ M^{-1} s^{-1}; initial values, $C_{A_0} = C_{B_0} = 1.4 \times 10^{-2}$ M, $I_0 = 5.8 \times 10^{-9}$ photons/(s·cm^2).

tion is hydrodynamically unstable and convections start. The values are Ra = 658, 1101, and 1708 for two free boundaries, one free and one rigid boundary, and two rigid boundaries, respectively.

In a multicomponent system, the situation is more complex. The stability of two-component systems is a much discussed problem in the hydrodynamic literature, where, usually, the two components are heat and salt. These systems are characterized by two Rayleigh numbers, one for each component, and the stability criteria for two opposing *linear* density gradients are known.[18] If $D_A < D_B$ and A is the unstable component, the condition for stability is

$$Ra_A + Ra_B < Ra_{critical} \tag{18}$$

and above the threshold (when $Ra_{critical}$ is negligible)

$$\frac{\alpha_A \Delta C_A}{\alpha_B \Delta C_B} < \frac{D_A}{D_B} \tag{19}$$

The above condition states that in a two-component solution hydrodynamic instability can evolve even when the overall density is *decreasing* upward. Heavy top on light bottom, therefore, is not a necessary condition for instability.

Coming back to the profiles of this study, there are some additional problems. First, the systems in consideration are not static, while the above criteria are based on the assumption that the concentration profiles are in a steady state. Secondly, even if we assume that we can "freeze" the system at any moment and examine its stability, the profiles presented here are not linear, and the gradients of the components expand over layers of different width. Stability analysis calculations for various nonlinear and nonmonotonic density profiles of one-component systems appear in the hydrodynamic literature,[19] but we are not aware of solutions for cases of multicomponent nonlinear gradients. It is worth mentioning that even for one component the transition from linear to nonlinear gradient can change the value of the critical Rayleigh number significantly.

While the effect of the expansion coefficients ratio on the hydrodynamic stability is quite obvious, the effect of the diffusion coefficients on the hydrodynamic stability is more complex. Since in our system both $\Delta\rho$ and Δh are determined by the diffusion coefficients, it is difficult to estimate their overall effect. For example, without a detailed stability analysis it is impossible to determine which profile, Figure 4b or 4c, will reach instability first.

The photochemical reaction of section 3.4 offers an opportunity to estimate the Rayleigh number of the system at the known onset time and compare it to the critical value. Using the fact that in this case the concentration gradients of all the components expand over about the same thickness and the fact that the diffusion coefficients of the reactants are almost equal, we can approximate the Rayleigh number of the solution by using eq 18 (by reducing the system to a two-component, reactants and product, system), neglecting for the moment the nonlinearity of the profiles. This crude calculation gives Rayleigh number values of 10^5–10^6 for times between 100 and 500 s and a value on the order of 10^3, i.e., on the order of the critical value (see above) at about 5 s after the reaction had begun. The discrepancy between experiment and calculation may be explained by the deviation from linearity of the profiles and by the above-mentioned "freezing" assumption. Quasi-steady-state calculations are justified only if the perturbations grow at a much faster rate than the profile develops. This might not be the case here: As was shown by Mahler et al.,[14] in systems where a sudden change of concentration or temperature occurs the onset time of convections is very much affected by the initial perturbations. Thus, in such systems the Rayleigh number cannot predict the onset time. It seems to us, therefore, that the quasi-stationary stability analysis approach might not be the right approach for these systems and that direct stimulation of the full chemical and hydrodynamic equations might be necessary in order to be able to compare theoretical to experimental results.

In all of the above examples, we considered only density profiles that are a direct result of the concentration gradients evolving during the reaction. We assumed no temperature gradients. In reality, the solution might be very sensitive to temperature gradients, which can be generated by the reaction enthalpy and which would be another cause for convections.

Despite all these hydrodynamic consideration difficulties, a main conclusion is at hand: A wide variety of interfacial reactions evolve density profiles very quickly which may lead to spontaneous convections. This in turn provides a mechanism for mixing which is faster than diffusion and should be taken into account when considering the rate of chemical reactions near an interface.

Acknowledgment. Supported by the Israel Space Agency through the National Council for R&D. We thank Dr. Michael Magen for many helpful discussions.

(18) Turner, J. S. *Buoyancy Effects in Fluids*; Cambridge University Press: New York, 1973; Chapter 8.

(19) Magen, M. The problem of localized thermal instability. Preprint, 1988. Whitehead, J. A.; Chen, M. M. *J. Fluid. Mech.* **1970**, *40*, 549.